Developmental Cell *13*

Supplemental Data

Stabilization of Overlapping Microtubules by Fission Yeast CLASP

Scott V. Bratman and Fred Chang

Supplemental Discussion

Is Cls1p a +TIP in Interphase Cells?

We discuss here differences of this study with a previous study by Grallert et al. (2006) on this same gene protein, *S. pombe* cls1p/peg1p. This previous paper concluded that cls1p is a +TIP that regulates interphase MT plus end dynamics in a dynein-dependent manner. In both *cls1* and *dhc1* (dynein heavy chain) mutants, they report that MT plus ends have a decrease in MT catastrophe rates, causing MTs to grow too long.

After extensive efforts, we have not visualized cls1p on MT plus ends and have not observed effects of *cls1* mutations on MT plus end dynamics. Cls1p was not detectable on growing MT plus ends (away from overlap zones), despite use of fusions with multiple GFPs or even overexpression; the sensitivity of our imaging system should allow us to visualize even very small numbers of cls1p (2-3 molecules). Our localization pattern is the same as shown by Grallert et al., but our dual time-lapse imaging with MTs or +TIP proteins demonstrates that these cytoplasmic dots do not represent growing MT plus ends. We have also not found a dynein-dependence for cls1p localization.

In addition, we have not been able to replicate the phenotypes of MT plus end dynamics in *cls1* and dynein mutants. Allelic difference cannot explain these effects, as we also examined the *peg1.1* allele (obtained from the Hagan lab) and the same allele (*cls1-32*; L747F) that was

isolated in our screen. We also did not see defects in catastrophe regulation in *cls1*Δ germinating spores (our unpublished observations).

While it was difficult for us to pinpoint specific sources of experimental differences, one likely source in measuring MT dynamics is the GFP-tubulin construct used in the analysis of the mutant phenotypes. GFP-α-tubulin fusions are not functional and thus have the potential to alter MT dynamic behavior, especially when expressed at high levels. Grallert et al. used strains in which an *nmt81:GFP-atb2* construct replaces the chromosomal *atb2*$^{+}$. In our studies, we used a construct that expresses low levels (~1% of α-tubulin) from a plasmid or another chromosomal locus, without disrupting the endogenous *atb2*$^{+}$ gene. Quantification of GFP-tubulin in these strains (Figures S6F and S6G) indicates that the construct used by Grallert et al. is expressed approximately two-fold higher than our *SV40:GFP-atb2* construct and the commonly used plasmid, pDQ105 (Ding et al., 1998). Factoring in the loss of the wild-type atb2p (a ~40% drop in total α-tubulin), the Grallert strains express less total α-tubulin and a significantly higher proportion of labeled α-tubulin.

The construct used by Grallert et al. has been noted previously to produce MT-related defects (Garcia et al., 2001; Kerres et al., 2007). In particular, we note that in the *nmt81:GFP-atb2* strains, anaphase spindles occasionally bend severely leading to premature spindle breakdown; this behavior is not seen in *SV40:GFP-atb2* strains. To further assess the effect of the GFP fusion on tubulin function, we combined the *GFP-atb2* alleles with the temperature-sensitive *alp14-1270* (TOG, X-MAP215 family) allele. Complete loss of atb2p function is synthetic lethal with *alp14-1270*, and *nmt81:GFP-atb2 alp14-1270* is sick with abnormal cell morphology at the permissive temperature (Garcia et al., 2001). In contrast, *SV40:GFP-atb2 alp14-1270* strain did not have any noticeable synthetic defects (Figure S6H), indicating that the *SV40:GFP-atb2* construct is less affected in tubulin function than *nmt81:GFP-atb2*.

Supplemental Experimental Procedures

Generation of *S. pombe* Strains

Oligonucleotides and plasmids used in this study are listed in Tables S2 and S3, respectively. To generate *cls1*Δ strains, the entire *cls1* ORF was replaced in a diploid with *ura4*$^+$ (Bahler et al., 1998) or the *natMX4* cassette (Goldstein and McCusker, 1999). For introducing C-terminal tags into the *cls1* locus, oligos osm375 and osm376 were used to amplify linear DNA from pFA6a-3GFP-kanMX6 (Wu et al., 2006) or pFA6a-13myc-kanMX6 (Bahler et al., 1998). C-terminal tags were integrated immediately preceding the stop codon of the *cls1* ORF without additional linker residues. Oligos oSB61 and oSB62 (no tag) or oligos oSB61 and oSB63 (GFP tag with $[gly\text{-}ala]_3$ linker) were used to introduce the *nmt1* promoter immediately upstream of the *cls1* ORF.

For the generation of *cls1*^{ts} alleles, pSB48 was first assembled in pBluescript (see below). Next, a ~5.5kb linear DNA fragment containing the 3' 827 codons of *cls1*, *nmt1* transcription termination, *ura4*$^+$, and the *cls1* 3'UTR was amplified by PCR from pSB48 with oligos oSB71 and oSB72; Taq polymerase (Roche) was used in eight separate PCR reactions under standard conditions to generate random point mutations (Zhou et al., 1991). This fragment was transformed into *S. pombe* strain SB445 (*cls1-mCFP:kanMX*), and colonies that grew on plates lacking uracil were screened for growth at 36ºC on plates containing phloxin B (Bio 101), which stains dead cells red. Single colonies that grew at 25ºC but not at 36ºC were screened for loss of G418-resistance and CFP fluorescence. To ensure homogeneity of the *cls1*^{ts} strains, colonies were streaked for single colonies and back-crossed to the wild-type strain FC420. The occurrence of a single integration event at the *cls1* locus was confirmed by tetrad analysis.

The GFP-α-tubulin strain FC1234 was constructed as follows. Plasmid pMP103 (Pardo and Nurse, 2005) contains *SV40:GFP-atb2*$^+$ in the *leu1*$^+$ integration vector, pJK148 (Keeney

and Boeke, 1994). pMP103 was linearized and stably integrated into the *leu1* locus of FC421. Specific integration into *leu1* was confirmed by back-crosses.

Plasmid Construction

For mutagenesis of *cls1*, pSB48 was constructed as follows. First, the *cls1* open reading frame was amplified from genomic DNA in two seqments (5' segment with oligos oSB49 and oSB52; 3' segment with oligos oSB50 and oSB51) by KOD polymerase (Novagen) and inserted by three-way ligation into the XhoI-BamHI sites of pREP4X (Forsburg, 1993) to create pSB37. Next, the following fragments were inserted into the EcoRI, HindIII, and XhoI sites, respectively, of pBluescript to generate pSB48: a 3.3kb fragment from pSB37 containing *cls1* sequences and the *nmt1* transcription termination; a 1.8kb fragment from pREP4X containing *ura4*$^+$; and ~0.6kb from the 3'UTR of *cls1* amplified from genomic DNA with oligos oSB67 and oSB68 by KOD polymerase.

To generate pSB62 (pREP41X-mRFP-atb2), the *atb2*$^+$ ORF was amplified by PCR with KOD polymerase from pDQ105 (Ding et al., 1998) with oligos oSB114 and oSB115 and inserted into the XhoI-BamHI sites of the pREP41X-mRFP vector, pSM526 (Martin and Chang, 2006). For imaging mRFP-α-tubulin, cells were grown at 25ºC in minimal media lacking thiamine for >24 hrs.

Plasmid pSB66, an *S. pombe* vector used for expression of cls1 fragments fused to the C-terminus of mCherry, was constructed from pREP42X by replacing the 1.2kb SphI-XhoI fragment containing the *nmt41* promoter with a 1.9kb fragment containing the *nmt1* promoter, mCherry, and a short $(GA)_3$ linker. This 1.9kb fragment was amplified from pKS394 (Snaith et al., 2005) by KOD polymerase with oligos oSB120 and oSB121.

Cls1p Overexpression

For induction of cls1p overexpression from the *nmt1* promoter, cells were first grown in liquid culture in the presence of thiamine, then washed three times and grown for 14-16 hrs at 30ºC in

minimal media lacking thiamine. We analyzed cells in these initial hours of induction, as prolonged overexpression was toxic to cells and prevented colony formation on plates.

Quantifying Numbers of Cls1p Molecules from Fluorescence Intensity Measurements

In order to determine the total number of cls1p molecules in a cell, we compared fluorescence intensities of cells expressing cls1-3GFP with those expressing cdc12-3GFP at endogenous levels, as described (Martin and Chang, 2006). Based on estimates of cdc12p (Wu and Pollard, 2005), we estimated that there are on average 516 cls1p molecules in an interphase cell (n=40) and 752 molecules in a mitotic cell (n=13). Similar numbers were found with the *S. cerevisiae* CLASP ortholog, Stu1p (Ghaemmaghami et al., 2003). Ratios of the intensities of single dots and the cell-wide signal was used to estimate the number of cls1p molecules per dot.

We estimated the number of MTs within the fission yeast mitotic spindle from a previous EM study (Ding et al., 1993). Excluding short non-overlapping MTs near spindle poles of anaphase spindles, the eleven spindles analyzed had between 8 and 45 MTs (mean=20±14; median=12). A comparison of means and medians of cls1p molecules and spindle MTs (means, 11 cls1p molecules per MT; medians, 18 cls1p molecules per MT) is in general agreement with our analysis of the interphase cls1p patch. Levels of cls1p overexpression were determined by comparing fluorescence intensities of cells overexpressing GFP-cls1p with cells expressing cls1-3GFP at endogenous levels, and multiplying by a factor of 3 to account for the different tags (Joglekar, Bloom, and Salmon, personal communication).

Quantification of α-Tubulin Levels

Relative levels of GFP-tubulin in cells were determined by fluorescence quantification and immunoblotting. Fluorescence intensities were compared in live cells between strains expressing GFP-atb2p from pDQ105 (repressed *nmt1* promoter; Ding et al., 1998), an integrated *SV40* promoter (this study), or a fully induced *nmt81* promoter (Garcia et al., 2001).

In the *nmt81:GFP-atb2* strain, the only atb2p in the cell is tagged with GFP; the other strains have exogenous GFP-atb2p that is expressed in addition to wild-type atb2p.

Levels in cell extracts of GFP-atb2p and total untagged α-tubulin (nda2p and atb2p) were determined by immunoblotting and scanning densitometry. All α-tubulins were detected with TAT-1 monoclonal antibodies. Monoclonal anti-actin antibodies (ab8224; Abcam) were used for loading control.

Coimmunoprecipitations

High-speed soluble extracts were prepared from mortal and pestle yeast extracts in CXS buffer (50mM Hepes pH7.0, 20mM KCl, 1mM $MgCl_2$, 2mM EDTA, protease inhibitors) by centrifugation at 45krpm for 30min in a TLA100 rotor (Beckman), and Triton X-100 was added to a final concentration of 0.1%. 175µL extract was added to 20µL sheep anti-mouse magnetic Dynabead slurry (Dynal) pre-bound (non-covalently) to 2µg monoclonal anti-myc (9E10; Santa Cruz Biotech) or monoclonal anti-HA antibodies (HA.11; Covance) and incubated for 2hr at 4ºC. The beads were washed once with CSX+100mM NaCl and four times with CSX+300mM NaCl. Samples were analyzed by SDS-PAGE and immunoblotting with monoclonal anti-HA or polyclonal anti-myc (A-14; Santa Cruz Biotech) antibodies.

In Vitro Binding Assay

MBP and MBP-ase1 were expressed in *E. coli* and affinity purified on an amylose resin (Clontech). GST-cls1_M and GST-cls1_C were expressed in *E. coli*, affinity purified on a glutathione resin (NEB), and eluted with 20mM reduced glutathione in 100mM Tris (pH8.7). Equivalent amounts of purified GST fusions were added to MBP- or MBP-ase1-coupled amylose resin in micro bio-spin columns (Biorad) and incubated for 2hr at 4ºC. The columns were washed five times with B buffer (20mM Tris [pH8.0], 20mM KCl, 130mM NaCl, 1mM $MgCl_2$, 2mM EDTA) and five times with B buffer + 0.05% NP-40. MBP fusions and any bound

proteins were then eluted from the amylose resin in 10mM maltose. Samples were analyzed by SDS-PAGE, coomassie staining, and immunoblotting with monoclonal anti-GST antibodies (Covance). For binding experiments, 20% and 40% of input was loaded onto gels for immunoblotting and coomassie staining, respectively.

Cls1p Domain Localization and Viability Assays

Cls1p was subdivided into five domains based on sequence characteristics and homology: the N-terminal HEAT-repeat region that is sufficient for MT stabilization when overexpressed (aa 1-500); the basic and serine-rich region (aa 501-604); the ase1p-binding domain (aa 605-812); a low complexity region with predicted coiled coils (aa 813-1196); and the C-terminal HEAT-repeat region (aa 1197-1462) that has homology to the kinetochore- and CLIP170-interacting region of mammalian CLASP.

cls1 gene fragments were amplified with KOD polymerase and inserted into the XhoI-BamHI sites of pSB66. Plasmids were introduced into the GFP-tubulin strains FC1234 (*cls1*$^{+}$ haploid) and SB575 (*cls1+/cls1*Δ*::natMX* diploid). Rescue of viability in *cls1*Δ*::natMX* was determined from the percent of haploid SB575 spores harboring the plasmid that were nourseothricin-resistant.

Protein Sequence Comparison and Analysis

Secondary structure prediction was performed using PredictProtein (Rost et al., 2004). Regions that are indicated as buried or exposed in the schematics (Figure S11) were simplified from the raw data. Predicted HEAT repeats and coiled coils were obtained from Pfam (v. 21.0). Criteria for basic, serine-rich domains: >40 aa, pI>10, >20% serines. Global pairwise sequence alignments were performed with ALIGN v. 2.0 (Myers and Miller, 1988), using the BLOSUM50 scoring matrix and gap penalties of –10/-2. Proteins included in these analyses: Sp Cls1p/Peg1p (Accession: O42874), Hs CLASP1 (Accession: Q7Z460), Sc Stu1p (Accession:

P38198), Sp Dis1p (Accession: Q09933), and Ce Zyg9 (Accession: O61442). The structure of the TOG3 domain of Ce Zyg9 is known (Al-Bassam et al., 2007).

Supplemental References

Al-Bassam, J., Larsen, N. A., Hyman, A. A., and Harrison, S. C. (2007). Crystal structure of a TOG domain: conserved features of XMAP215/Dis1-family TOG domains and implications for tubulin binding. Structure *15*, 355-362.

Bahler, J., Wu, J. Q., Longtine, M. S., Shah, N. G., McKenzie, A., 3rd, Steever, A. B., Wach, A., Philippsen, P., and Pringle, J. R. (1998). Heterologous modules for efficient and versatile PCR-based gene targeting in Schizosaccharomyces pombe. Yeast *14*, 943-951.

Ding, D. Q., Chikashige, Y., Haraguchi, T., and Hiraoka, Y. (1998). Oscillatory nuclear movement in fission yeast meiotic prophase is driven by astral microtubules, as revealed by continuous observation of chromosomes and microtubules in living cells. J Cell Sci *111 (Pt 6)*, 701-712.

Ding, D. Q., Chikashige, Y., Haraguchi, T., and Hiraoka, Y. (1998). Oscillatory nuclear movement in fission yeast meiotic prophase is driven by astral microtubules, as revealed by continuous observation of chromosomes and microtubules in living cells. J Cell Sci *111 (Pt 6)*, 701-712.

Ding, R., McDonald, K. L., and McIntosh, J. R. (1993). Three-dimensional reconstruction and analysis of mitotic spindles from the yeast, Schizosaccharomyces pombe. J Cell Biol *120*, 141-151.

Forsburg, S. L. (1993). Comparison of Schizosaccharomyces pombe expression systems. Nucleic Acids Res *21*, 2955-2956.

Garcia, M. A., Vardy, L., Koonrugsa, N., and Toda, T. (2001). Fission yeast ch-TOG/XMAP215 homologue Alp14 connects mitotic spindles with the kinetochore and is a component of the Mad2-dependent spindle checkpoint. Embo J *20*, 3389-3401.

Ghaemmaghami, S., Huh, W. K., Bower, K., Howson, R. W., Belle, A., Dephoure, N., O'Shea, E. K., and Weissman, J. S. (2003). Global analysis of protein expression in yeast. Nature *425*, 737-741.

Glynn, J. M., Lustig, R. J., Berlin, A., and Chang, F. (2001). Role of bud6p and tea1p in the interaction between actin and microtubules for the establishment of cell polarity in fission yeast. Curr Biol *11*, 836-845.

Goldstein, A. L., and McCusker, J. H. (1999). Three new dominant drug resistance cassettes for gene disruption in Saccharomyces cerevisiae. Yeast *15*, 1541-1553.

Grallert, A., Beuter, C., Craven, R. A., Bagley, S., Wilks, D., Fleig, U., and Hagan, I. M. (2006). S. pombe CLASP needs dynein, not EB1 or CLIP170, to induce microtubule instability and slows polymerization rates at cell tips in a dynein-dependent manner. Genes Dev *20*, 2421-2436.

Keeney, J. B., and Boeke, J. D. (1994). Efficient targeted integration at *leu1-32* and *ura4-294* in Schizosaccharomyces pombe. Genetics *136*, 849-856.

Kerres, A., Jakopec, V., and Fleig, U. (2007). The Conserved Spc7 Protein Is Required for Spindle Integrity and Links Kinetochore Complexes in Fission Yeast. Mol Biol Cell.

Lemos, C. L., Sampaio, P., Maiato, H., Costa, M., Omel'yanchuk, L. V., Liberal, V., and Sunkel, C. E. (2000). Mast, a conserved microtubule-associated protein required for bipolar mitotic spindle organization. Embo J *19*, 3668-3682.

Loiodice, I., Staub, J., Setty, T. G., Nguyen, N. P., Paoletti, A., and Tran, P. T. (2005). Ase1p organizes antiparallel microtubule arrays during interphase and mitosis in fission yeast. Mol Biol Cell *16*, 1756-1768.

Maiato, H., Fairley, E. A., Rieder, C. L., Swedlow, J. R., Sunkel, C. E., and Earnshaw, W. C. (2003). Human CLASP1 is an outer kinetochore component that regulates spindle microtubule dynamics. Cell *113*, 891-904.
Martin, S. G., and Chang, F. (2006). Dynamics of the formin for3p in actin cable assembly. Curr Biol *16*, 1161-1170.
Nakaseko, Y., Nabeshima, K., Kinoshita, K., and Yanagida, M. (1996). Dissection of fission yeast microtubule associating protein p93Dis1: regions implicated in regulated localization and microtubule interaction. Genes Cells *1*, 633-644.
Pardo, M., and Nurse, P. (2005). The nuclear rim protein Amo1 is required for proper microtubule cytoskeleton organisation in fission yeast. J Cell Sci *118*, 1705-1714.
Pasqualone, D., and Huffaker, T. C. (1994). *STU1*, a suppressor of a beta-tubulin mutation, encodes a novel and essential component of the yeast mitotic spindle. J Cell Biol *127*, 1973-1984.
Rost, B., Yachdav, G., and Liu, J. (2004). The PredictProtein server. Nucleic Acids Res *32*, W321-326.
Snaith, H. A., Samejima, I., and Sawin, K. E. (2005). Multistep and multimode cortical anchoring of tea1p at cell tips in fission yeast. Embo J *24*, 3690-3699.
Yamashita, A., Sato, M., Fujita, A., Yamamoto, M., and Toda, T. (2005). The roles of fission yeast ase1 in mitotic cell division, meiotic nuclear oscillation, and cytokinesis checkpoint signaling. Mol Biol Cell *16*, 1378-1395.
Yin, H., You, L., Pasqualone, D., Kopski, K. M., and Huffaker, T. C. (2002). Stu1p is physically associated with beta-tubulin and is required for structural integrity of the mitotic spindle. Mol Biol Cell *13*, 1881-1892.
Zhou, Y. H., Zhang, X. P., and Ebright, R. H. (1991). Random mutagenesis of gene-sized DNA molecules by use of PCR with Taq DNA polymerase. Nucleic Acids Res *19*, 6052.

Table S1. Strains Used in This Study

Strain	Genotype	Source/Reference
FC420	*h+ leu1- ura4- ade6-*	Chang Lab
FC421	*h- leu1- ura4- ade6-*	Chang Lab
FC1165	*h- ase1-YFP:kanMX leu1- ura4-*	Yamashita et al., 2005
FC1188	*h- mto1-GFP:kanMX leu1- ura4- ade6-*	Chang Lab
FC1234	*h- leu1-::SV40:GFP-atb2:leu1+ ura4- ade6-*	This study
FC1597	*h- kanMX:nmt81:GFP-atb2 leu1-*	Garcia et al., 2001
FC1890	*h+ alp14-1270 leu-*	Garcia et al., 2001
SB354	*h- cls1-3GFP:kanMX leu1- ura4- ade6-*	This study
SB371	*h- kanMX:nmt1:cls1 leu1-::SV40:GFP-atb2:leu1+ ura4- ade6-*	This study
SB377	*tip1::kanMX cls1-3GFP:kanMX*	This study
SB378	*tea2::his3+ cls1-3GFP:kanMX leu1- ura4- ade6-*	This study
SB390	*h- cls1-3GFP:kanMX leu1- ura4- ade6- pRL74*	This study
SB397	*ase1::kanMX leu1-::SV40:GFP-atb2:leu1+ ura4-*	This study
SB399	*tea1::ura4+ cls1-3GFP:kanMX ura4-*	This study
SB403	*tip1-CFP:kanMX cls1-3GFP:kanMX leu1- ura4- ade6-*	This study
SB405	*mto1::KanMX leu1-::SV40:GFP-atb2:leu1+ ura4- ade6-*	This study
SB411	*mal3::his3+ cls1-3GFP:kanMX leu1- ura4- ade6-*	This study
SB416	*kanMX:nmt1:GFP-cls1 leu1- ura4- ade6-*	This study
SB428	*cls1::ura4+/cls1+ leu1-::SV40:GFP-atb2:leu1+/leu1- ura4-/ura4- ade6-M216/ade6-M210*	This study
SB445	*h+ cls1-mCFP:kanMX leu1-::SV40:GFP-atb2:leu1+ ura4- ade6-*	This study
SB466	*cls1-9:ura4+ leu1-::SV40:GFP-atb2:leu1+ ura4- ade6-*	This study
SB468	*cls1-19:ura4+ leu1-::SV40:GFP-atb2:leu1+ ura4- ade6-*	This study
SB485	*h- cls1-26:ura4+ leu1-::SV40:GFP-atb2:leu1+ ura4- ade6-*	This study
SB488	*h- cls1-28:ura4+ leu1-::SV40:GFP-atb2:leu1+ ura4- ade6-*	This study
SB491	*h- cls1-29:ura4+ leu1-::SV40:GFP-atb2:leu1+ ura4- ade6-*	This study
SB493	*h- cls1-31:ura4+ leu1-::SV40:GFP-atb2:leu1+ ura4- ade6-*	This study
SB495	*h- cls1-32:ura4+ leu1-::SV40:GFP-atb2:leu1+ ura4- ade6-*	This study
SB497	*h- cls1-34:ura4+ leu1-::SV40:GFP-atb2:leu1+ ura4- ade6-*	This study
SB499	*h- cls1-35:ura4+ leu1-::SV40:GFP-atb2:leu1+ ura4- ade6-*	This study
SB501	*h- cls1-36:ura4+ leu1-::SV40:GFP-atb2:leu1+ ura4- ade6-*	This study
SB503	*h- cls1-37:ura4+ leu1-::SV40:GFP-atb2:leu1+ ura4- ade6-*	This study
SB505	*h- cls1-38:ura4+ leu1-::SV40:GFP-atb2:leu1+ ura4- ade6-*	This study
SB507	*h- cls1-40:ura4+ leu1-::SV40:GFP-atb2:leu1+ ura4- ade6-*	This study
SB512	*h+ mal3::his3+ kanMX:nmt1:cls1 leu1-::SV40:GFP-atb2:leu1+ ura4-*	This study
SB514	*tip1::kanMX kanMX:nmt1:cls1 leu1-::SV40:GFP-atb2:leu1+*	This study
SB515	*mto1::kanMX kanMX:nmt1:cls1 leu1-::SV40:GFP-atb2:leu1+ ura4- ade6-*	This study
SB516	*h- ase1::kanMX kanMX:nmt1:cls1 leu1-::SV40:GFP-atb2:leu1+ ura4-*	This study
SB524	*mto1::kanMX cls1-36:ura4+ leu1-::SV40:GFP-atb2:leu1+ ura4- ade6-*	This study
SB533	*mto1-GFP:kanMX cls1-36:ura4+ leu1- ura4- ade6-*	This study
SB553	*ase1-YFP:kanMX cls1-28:ura4+ leu1- ura4-*	This study
SB565	*ase1-mCherry:natMX leu1-::SV40:GFP-atb2:leu1+ ura4- ade6-*	This study
SB575	*cls1::natMX/cls1+ leu1-::SV40:GFP-atb2:leu1+/leu1- ura4-/ura4- ade6-M216/ade6-M210*	This study
SB591	*h- cls1-3GFP:kanMX leu1-32 leu1- ura4- ade6- pSB62*	This study
SB603	*cls1-myc$_{13}$:kanMX ase1-HA$_3$:kanMX leu1- ura4- ade6-*	This study
SB617	*ase1-HA$_3$:kanMX leu1- ura4- ade6-*	This study
SB618	*cls1-myc$_{13}$:kanMX leu1- ura4- ade6-*	This study
SB632	*nda3-311 cls1-3GFP:kanMX ndc80-CFP:kanMX leu1- ura4-*	This study
SB633	*h+ cut12-CFP:kanMX cls1-3GFP:kanMX leu1- ura4-*	This study
SB635	*dhc1::kanMX cls1-3GFP:kanMX*	This study
SB636	*dhc1::kanMX leu1-::SV40:GFP-atb2:leu1+ ura4- ade6-*	This study
SB637	*dhc1::kanMX kanMX:nmt1:cls1 leu1-::SV40:GFP-atb2:leu1+ ura4- ade6-*	This study
SB716	*h- ase1[Δ665-731]:kanMX leu1-::SV40:GFP-atb2:leu1+ ura4- ade6-*	This study

SB718	*peg1.1 leu1-::SV40:GFP-atb2:leu1+ ura4- ade6-*	This study
SB725	*ase1[Δ665-731]:kanMX cls1-3GFP:kanMX leu1- ura4- ade6-*	This study
SB730	*ase1[Δ665-731]-mCherry:kanMX leu1-::SV40:GFP-atb2:leu1+ ura4- ade6-*	This study
SB737	*cls1-36:ura4+ klp5::ura4+ klp6::his3+ leu1- ura4- ade6-*	This study

Table S2. Oligos Used in This Study

Name	Sequence (5'→3')
osm375	TCAATATTGGGAGGATTAAATGAAGGACAAAGGCTTCTTTTCATGCATTATTTAAAGATGA AGTCTGATGAAAAGAATCGGATCCCCGGGTTAATTAA
osm376	AAAAGGAGCAGAGGAGGCAGTAGCGGAAGCTTCTTCTTGCATGCATAAGTTGAAGACATT AACAGGTTTGAGCGTATAGAATTCGAGCTCGTTTAAAC
oSB49	CGTACCCTCGAGATGGCGGATAAGGATGCGC
oSB50	TACGCGGATCCCTAATTCTTTTCATCAGACTTC
oSB51	CTTGGAGCAAGCAGGATGC
oSB52	CCTTTGCCATGTGGTACTAGC
oSB61	GCGAGTTTTTAATATTCTCTTCGCAAACAACGCTTCACGTTTCTCTTGTTTCGCTCGTTTC ATCAATATATTTGTAATTGGAATTCGAGCTCGTTTAAAC
oSB62	GTATATAGATGAAAGCTTTAGAATTTCATACCATTACTTTTAAGGAACTTTAAAAAATCTTG CGCATCCTTATCCGCCATGATTTAACAAAGCGACTATA
oSB63	TAGAATTTCATACCATTACTTTTAAGGAACTTTAAAAAATCTTGCGCATCCTTATCCGCCAT TGCTCCGGCTCCAGCACCTTTGTATAGTTCATCCATGC
oSB67	TACCGCTCGAGTTAGTATACGCTCAAACCTGTTAATGTC
oSB68	GCTAACAAGGTCCATTGCCCG
oSB71	TCGTCCAACTTAACAGATGCGC
oSB72	GCTAACAAGGTCCATTGCCCG
oSB114	GCGCTCGAGCATGAGAGAGATCATTTCCATTC
oSB115	CACGGATCCTTAGTACTCTTCTTCCATGTA
oSB120	GAGGCATGCCGCCATAAAAGACAGAATAAGTCATCAGC
oSB121	GAGCTCGAGTGCTCCGGCTCCAGCACCCTTGTACAGCTCGTCCATGC

Table S3. Plasmids Used in This Study

Name	Description	Selection Markers	Reference
pRL74	pREP4X-CFP-atb2	amp; ura4$^+$	Glynn et al., 2001
pDQ105	pREP1-GFP-atb2	amp; LEU2	Ding et al., 1998
pSB62	pREP41X-mRFP-atb2	amp; LEU2	
pSB37	pREP4X-*cls1*$^+$	amp; ura4$^+$	
pSB69	pMal	amp; ---	
pSB72	pMal-ase1(1-731)	amp; ---	
pSB78	pGEX-cls1_M(501-1196)	amp; ---	
pSB79	pGEX-cls1_C(813-1462)	amp; ---	
pSB32	pGBDK (C1)	kan; TRP1	
pSB99	pGBD-ase1(1-731)	kan; TRP1	
pSB100	pGBD-cls1_N(1-604)	kan; TRP1	
pSB101	pGBD-cls1_M(501-1196)	kan; TRP1	
pSB102	pGBD-cls1_C(813-1462)	kan; TRP1	
pSB116	pGBD-ase1(1-467)	kan; TRP1	
pSB117	pGBD-ase1(239-579)	kan; TRP1	
pSB118	pGBD-ase1(468-731)	kan; TRP1	
pSB144	pGBD-ase1(1-579)	kan; TRP1	
pSB145	pGBD-ase1(1-626)	kan; TRP1	
pSB146	pGBD-ase1(1-664)	kan; TRP1	
pSB52	pGAD (C1)	amp; LEU2	
pSB87	pGAD-ase1(1-731)	amp; LEU2	
pSB88	pGAD-cls1_N(1-604)	amp; LEU2	
pSB89	pGAD-cls1_M(501-1196)	amp; LEU2	
pSB90	pGAD-cls1_C(813-1462)	amp; LEU2	
pSB113	pGAD-cls1(605-1196)	amp; LEU2	
pSB114	pGAD-cls1(813-1196)	amp; LEU2	
pSB112	pGAD-cls1(605-812)	amp; LEU2	
pSB108	pGAD-cls1-26(605-812)	amp; LEU2	
pSB109	pGAD-cls1-28(605-812)	amp; LEU2	
pSB110	pGAD-cls1-29(605-812)	amp; LEU2	
pSB111	pGAD-cls1-36(605-812)	amp; LEU2	
pSB66	pNmt-mCherry	amp; ura4$^+$	
pSB119	pNmt-mCherry-cls1(1-500)	amp; ura4$^+$	
pSB120	pNmt-mCherry-cls1(1-604)	amp; ura4$^+$	
pSB121	pNmt-mCherry-cls1(1-812)	amp; ura4$^+$	
pSB122	pNmt-mCherry-cls1(1-1196)	amp; ura4$^+$	
pSB123	pNmt-mCherry-cls1(1-1462)	amp; ura4$^+$	
pSB124	pNmt-mCherry-cls1(501-604)	amp; ura4$^+$	
pSB125	pNmt-mCherry-cls1(501-812)	amp; ura4$^+$	
pSB126	pNmt-mCherry-cls1(501-11196)	amp; ura4$^+$	
pSB127	pNmt-mCherry-cls1(501-1462)	amp; ura4$^+$	
pSB128	pNmt-mCherry-cls1(605-812)	amp; ura4$^+$	
pSB129	pNmt-mCherry-cls1(605-1196)	amp; ura4$^+$	
pSB130	pNmt-mCherry-cls1(605-1462)	amp; ura4$^+$	
pSB131	pNmt-mCherry-cls1(813-1196)	amp; ura4$^+$	
pSB132	pNmt-mCherry-cls1(813-1462)	amp; ura4$^+$	
pSB133	pNmt-mCherry-cls1(1197-1462)	amp; ura4$^+$	
pSB135	pNmt-mCherry-cls1(1-604,813-1462)	amp; ura4$^+$	
pSB136	pNmt-mCherry-cls1(1-812,1197-1462)	amp; ura4$^+$	
pSB139	pNmt-mCherry-cls1(1-264)	amp; ura4$^+$	
pSB140	pNmt-mCherry-cls1(219-500)	amp; ura4$^+$	
pSB143	pNmt-mCherry-cls1(1-500,605-1462)	amp; ura4$^+$	

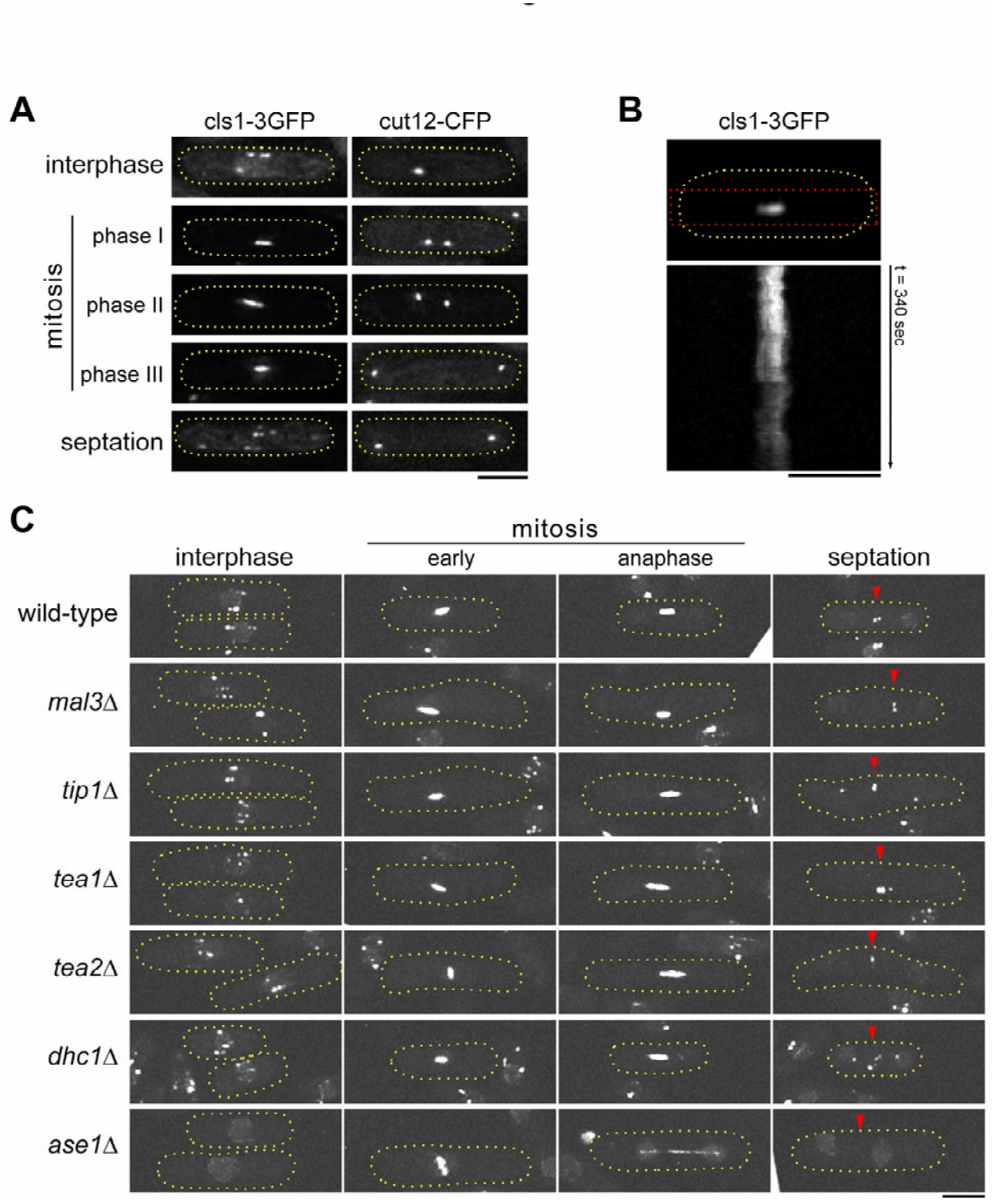

Figure S1. Cls1p Localization through the Cell Cycle

(A) Cls1-3GFP (left panels) in the cell cycle stages indicated. Cell cycle stage was determined by cut12-CFP localization (right panels) and DIC images (not shown). In interphase, one cls1p

dot colocalizes with cut12p at the SPB. Images are maximum projections of deconvolved stacks. Scale bar: 5µm.

(B) Mitotic cell expressing cls1-3GFP. Top, a single-plane confocal image. Bottom, kymograph of red-boxed region—constructed from time-lapse images (0.25 fps)—showing cls1p movements within the spindle midzone region.

(C) Cls1-3GFP localization through the cell cycle in mutant strains as indicated. Maximum projection confocal images are shown. Brightness levels in were increased to show dim signals. Red arrowheads mark the site of the developing septum. Cell cycle stage was determined by bright-field images and Hoechst 33342 staining (not shown). The cls1p dots are generally in the vicinity of the nucleus and not at cell tips. The localization pattern is unchanged in all mutants except for *ase1*Δ. The residual cls1p association with the spindle in *ase1*Δ mutants may explain why *ase1*Δ mutants have a less severe mitotic defect than *cls1* mutants (Loiodice et al., 2005; Yamashita et al., 2005).

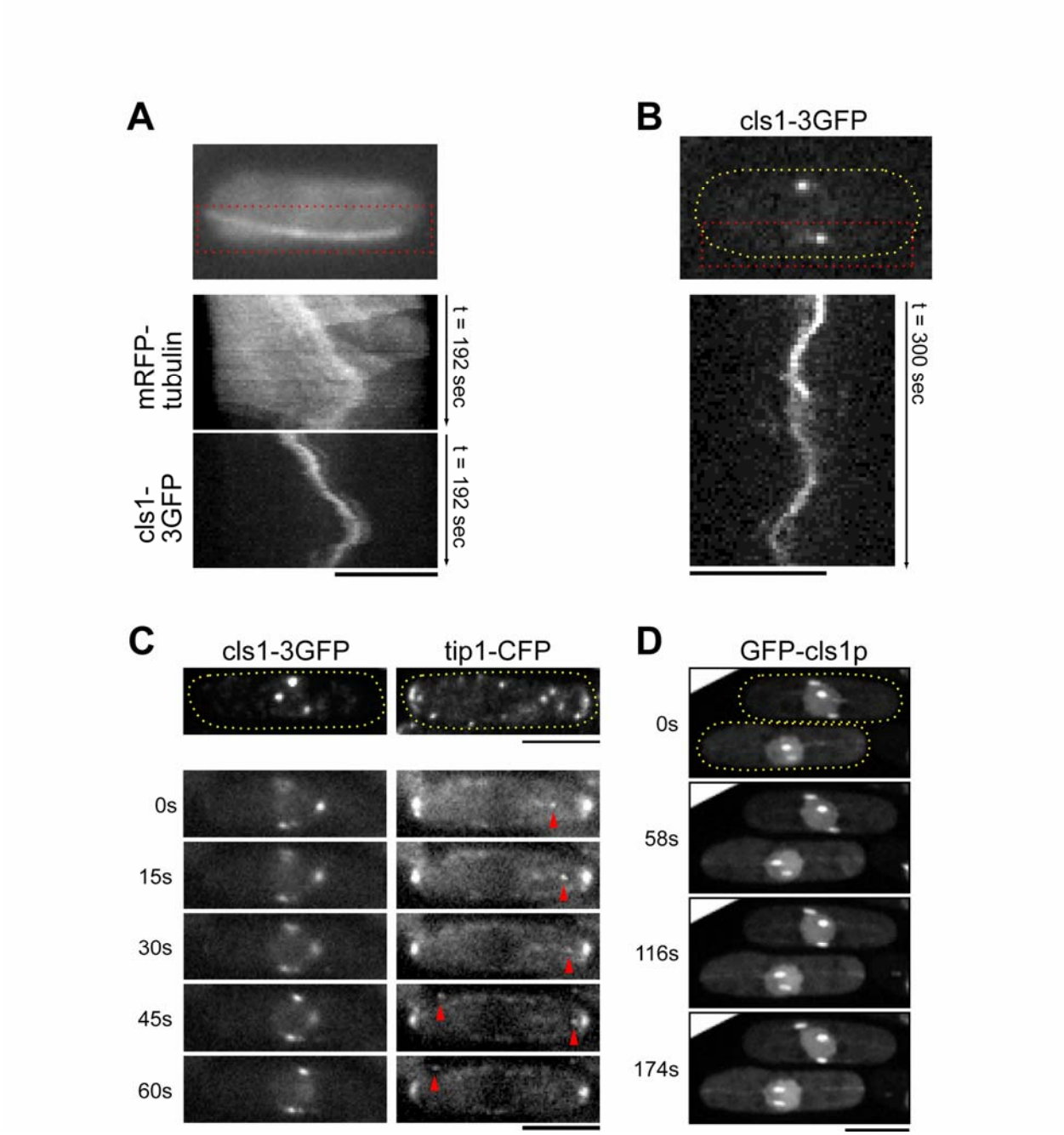

Figure S2. Cls1p Dynamics within Interphase MT Bundles

(A) Interphase cell expressing cls1-3GFP and mRFP-tubulin. Top, a single-plane image of mRFP-tubulin. Bottom, kymographs of red-boxed region—constructed from time-lapse images (0.25 fps)—showing persistent association of multiple cls1-3GFP dots within the MT overlap zone. Scale bar: 5μm.

(B) Interphase cell expressing cls1-3GFP. Top, a single-plane confocal image. Bottom, kymograph of red-boxed region—constructed from time-lapse images (0.25 fps)—showing cls1p movements within a single MT bundle. Some cls1p dots moved relative to each other, occasionally merging together or splitting into two, while others remained a fixed distance from each other for long periods (A). Some of the dots had relatively long lifetimes (>5 min), while others were short-lived (<1 min).

(C) Interphase cell expressing cls1-3GFP and tip1-CFP. Top, a maximum projection image. The localization patterns of these proteins do not overlap. Bottom, time-lapse images in a single focal plane showing cls1-3GFP movement around the nucleus and tip1-CFP dots on growing MT plus ends (arrowheads).

(D) GFP-cls1p moderately overexpressed from an integrated full-strength *nmt1* promoter repressed with thiamine. At these levels, cls1p strongly stains dots near the nucleus that are presumably within MT overlap zones. Cls1p can also be seen diffusely within the nucleus and dimly along the rest of the MT bundles without accumulation at plus ends. Maximum projection confocal images are shown.

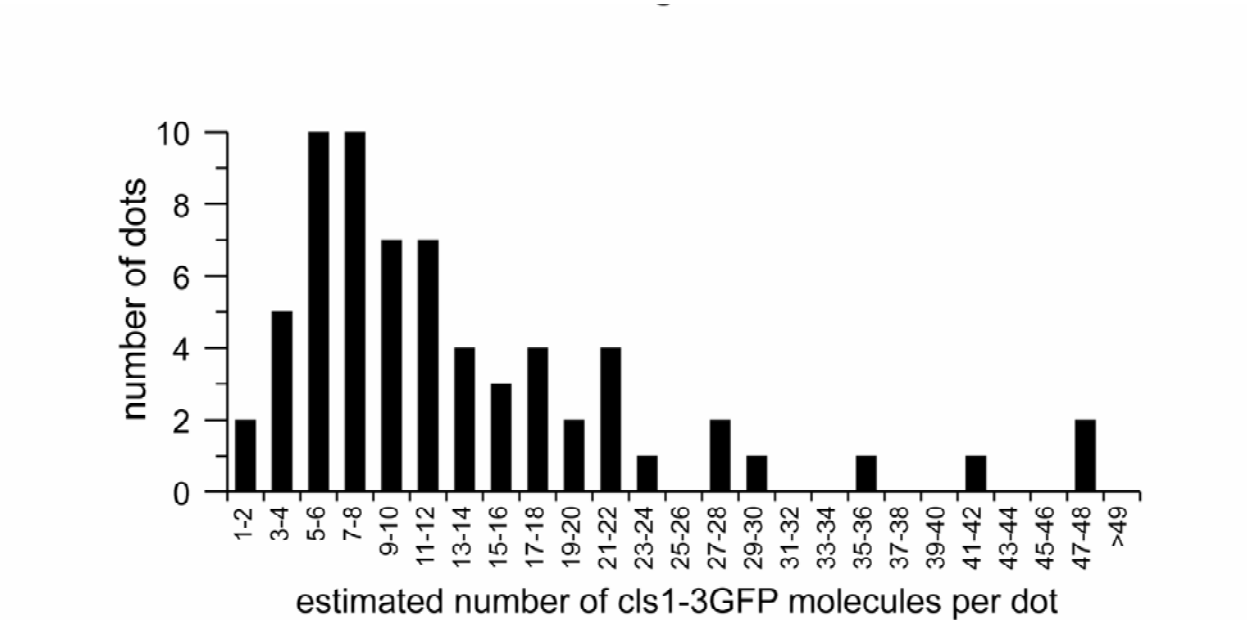

Figure S3. Quantification of cls1-3GFP Fluorescence Intensity

Histogram of the number of cls1-3GFP molecules that are estimated to be in a single dot observed in interphase cells. Average values are 13±10 (mean±S.D.) and 10 (median) molecules of cls1-3GFP per dot (n=66 dots).

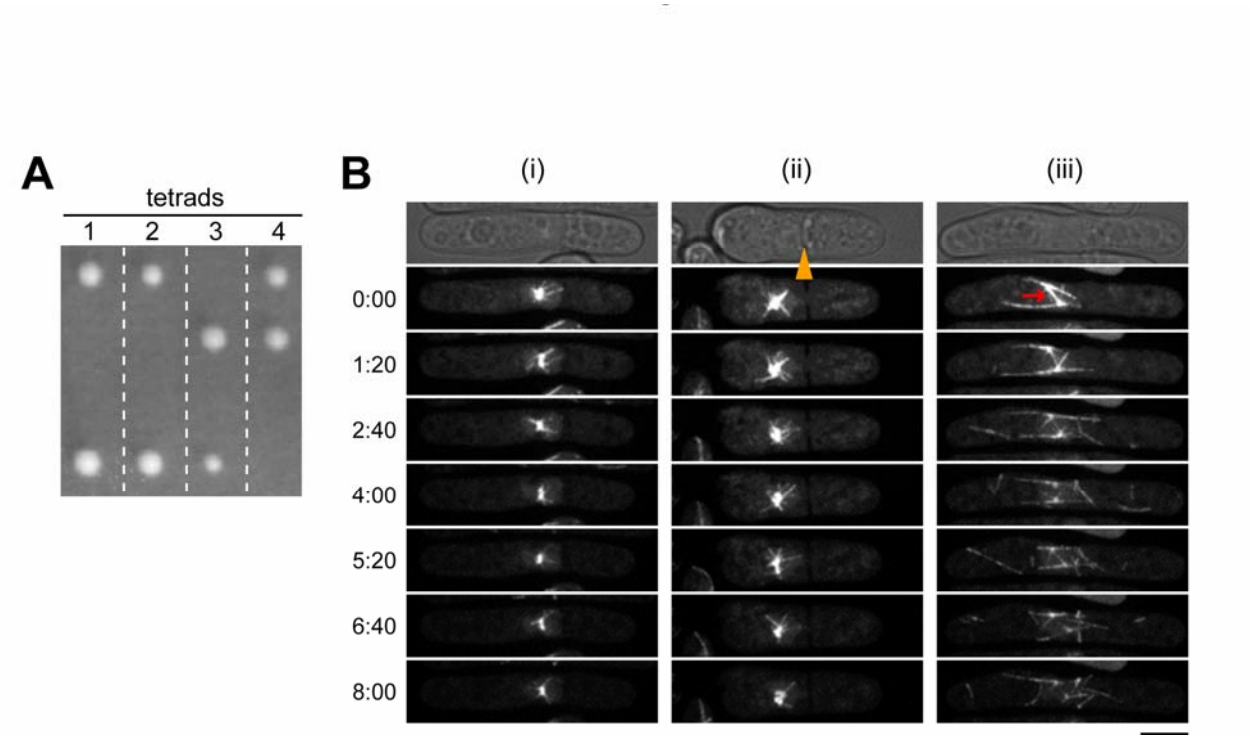

Figure S4. *cls1*Δ Cells Have Severe Mitotic Spindle Defects

(A) *cls1* is an essential gene. Tetrads of spores derived from *cls1*Δ/*cls1*$^{+}$ diploids were allowed to germinate on rich media plates. Only the two *cls1*$^{+}$ spores of each tetrad formed colonies.

(B) Three examples of defective spindles observed in germinated *cls1*Δ spores: (i) a monopolar spindle in a non-septated cell; (ii) a monopolar spindle in a septated cell (septum indicated by orange arrowhead); (iii) failed spindle elongation in which intra-nuclear interpolar MTs (red arrow) disappear even as cytoplasmic astral MTs are robust. Maximum projection confocal images of GFP-tubulin are shown. Time is in min:sec. Scale bars: 5µm.

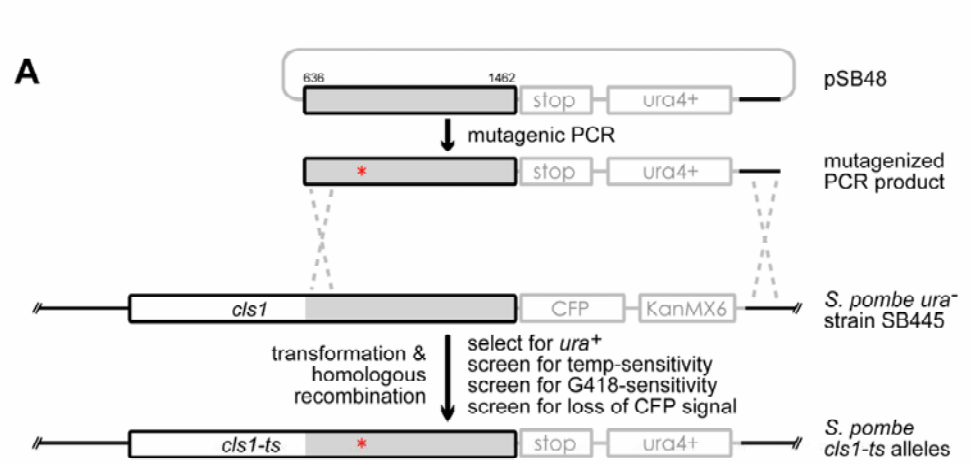

B

cls1-ts allele	mutations	growth on rich medium at: 25ºC	30ºC	33ºC	36ºC
cls1-9	L800S, T1368A	+	+	+	–
cls1-19	L747H, G888R	+	+	+	–
cls1-26	L747H	+	+	+	–
cls1-28	L797P	+	+/-	–	–
cls1-29	W746R	+	+	+/-	–
cls1-31	not determined	+	+	+	–
cls1-32	L747F	+	+	+	–
cls1-34	W746R, L1439S	+	+/-	–	–
cls1-35	W746R	+	+	+/-	–
cls1-36	I739T, D804V, E946K, I1277M	+	–	–	–
cls1-37	L797P	+	+/-	–	–
cls1-38	L800S, F997S	+	+	+	–
cls1-40	L747H	+	+	+	–

C

```
                731                                                   810
cls1p      FNTNQKRLIIHGCLLWLKEISDTKLNQLENKPFFVTDKLRYYSSKILAMTAKTKLTSKNWIPLSGLLFSLRAHDTFMFDG
cls1-26p   FNTNQKRLIIHGCLLWHKEISDTKLNQLENKPFFVTDKLRYYSSKILAMTAKTKLTSKNWIPLSGLLFSLRAHDTFMFDG
cls1-28p   FNTNQKRLIIHGCLLWLKEISDTKLNQLENKPFFVTDKLRYYSSKILAMTAKTKLTSKNWIPLSGLPFSLRAHDTFMFDG
cls1-29p   FNTNQKRLIIHGCLLRLKEISDTKLNQLENKPFFVTDKLRYYSSKILAMTAKTKLTSKNWIPLSGLLFSLRAHDTFMFDG
cls1-32p   FNTNQKRLIIHGCLLWFKEISDTKLNQLENKPFFVTDKLRYYSSKILAMTAKTKLTSKNWIPLSGLLFSLRAHDTFMFDG
cls1-36p   FNTNQKRLTIHGCLLWLKEISDTKLNQLENKPFFVTDKLRYYSSKILAMTAKTKLTSKNWIPLSGLLFSLRAHVTFMFDG
cls1-38p   FNTNQKRLIIHGCLLWLKEISDTKLNQLENKPFFVTDKLRYYSSKILAMTAKTKLTSKNWIPLSGLLFSSRAHDTFMFDG
                    *       **                                          *  *   *
```

Figure S5. Generation of *cls1^{ts}* Alleles

(A) Schematic describing the generation of point mutations in *cls1* by PCR-mediated random mutagenesis, and the incorporation of these mutations by homologous recombination.

(B) Missense mutations identified in the *cls1^{ts}* alleles. The restrictive temperatures of the *cls1^{ts}* alleles varied, but all were ts-lethal at 36ºC.

(C) Missense mutations in the *cls1^{ts}* alleles found between residues 731 and 810 in cls1p. All *cls1^{ts}* alleles contained mutations in this region.

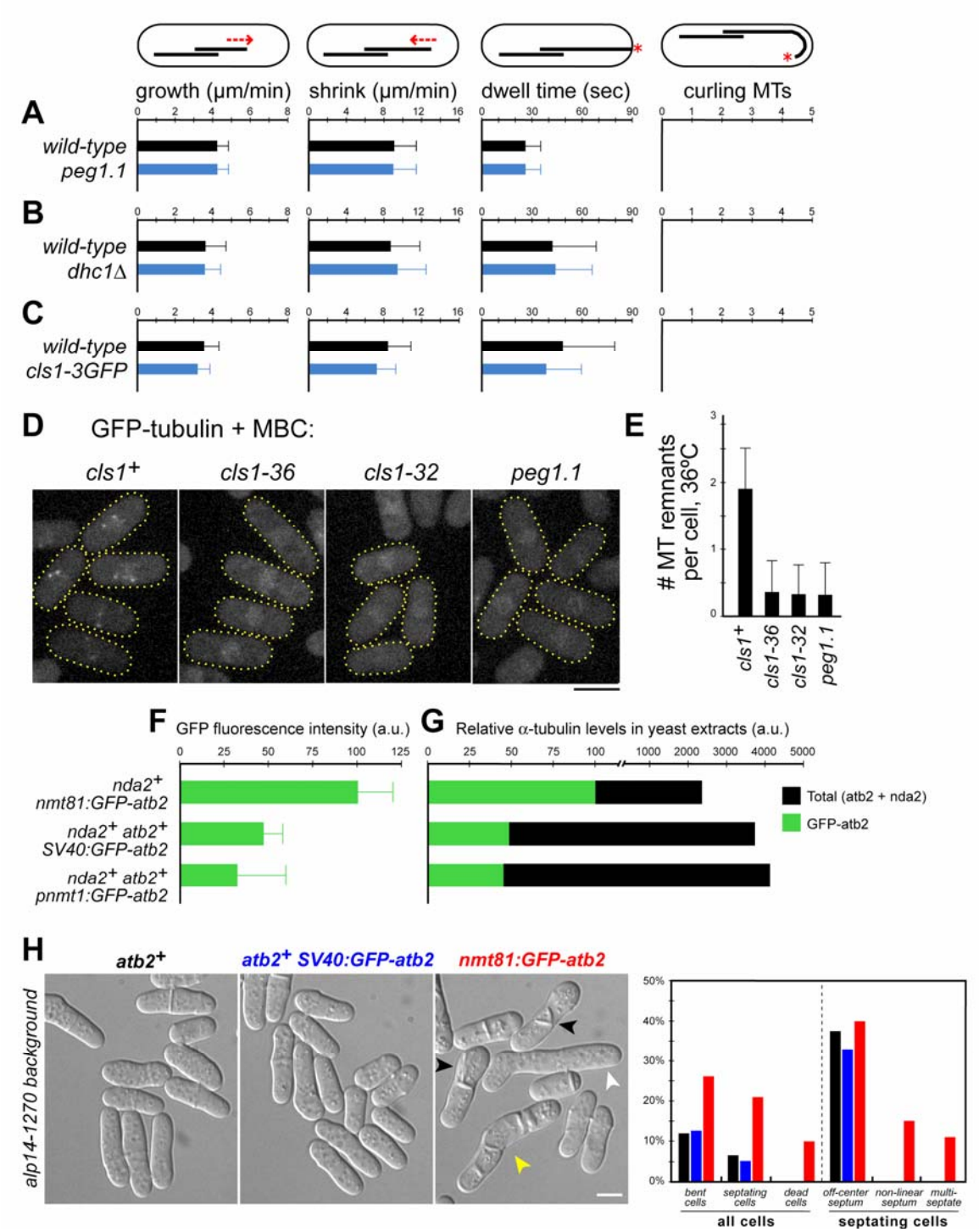

Figure S6. Interphase MTs in *peg1.1*, *dhc1*Δ, and *cls1-3GFP*

(A-C) Quantification of interphase MT plus end behavior. Plus end growth rates, shrinkage rates, and dwell times at cell tips (n=20 for each strain) were quantified from time-lapse maximum projection confocal images. There were no statistically significant differences in these

measurements. For each strain, no MTs were seen curling around cell tips in >20 cells imaged for 6 min. Strains in (A) express GFP-tubulin from an integrated, fully induced *nmt81* promoter (Grallert et al., 2006) and were imaged at the restrictive temperature (36ºC).

(D) Cells expressing GFP-tubulin from an integrated SV40 promoter were grown at 25˚C, and then treated with 25µg/mL MBC and shifted to 36ºC for 10 min. Maximum projection confocal images are shown. Scale bar: 5µm.

(E) Quantification of the number of stable MT remnants in MBC-treated cells at 36ºC (n>50 cells for each strain).

(F,G) Quantification of α-tubulin levels in three GFP-tubulin strains. Genotypes are indicated for both *nda2* (essential α-tubulin) and *atb2* (non-essential α-tubulin). Strains were grown in minimal media lacking thiamine (*nmt81:GFP-atb2* and *SV40:GFP-atb2*) or containing thiamine (*pnmt1:GFP-atb2*). All values are relative to GFP-atb2p levels in the *nmt81:GFP-atb2* strain, which is arbitrarily given a value of 100.

(F) Quantification of relative GFP-atb2p fluorescence intensities. n>80 cells for each strain.

(G) Quantification of GFP-atb2p and total α-tubulin levels in yeast extracts.

(H) The *nmt81:GFP-atb2*, but not *SV40:GFP-atb2*, is synthetic sick with *alp14-1270*. The indicated strains in the *alp14-1270* background were grown in minimal media lacking thiamine at 25ºC. From DIC images, >100 cells from each strain were scored for defects in cell shape and septum morphology. Cells with multiple septa (white arrowhead) or a non-linear septum (black arrowheads), and abnormally long cells (yellow arrowhead) were only seen in the *nmt81:GFP-atb2 alp14-1270* strain.

Error bars indicate SD.

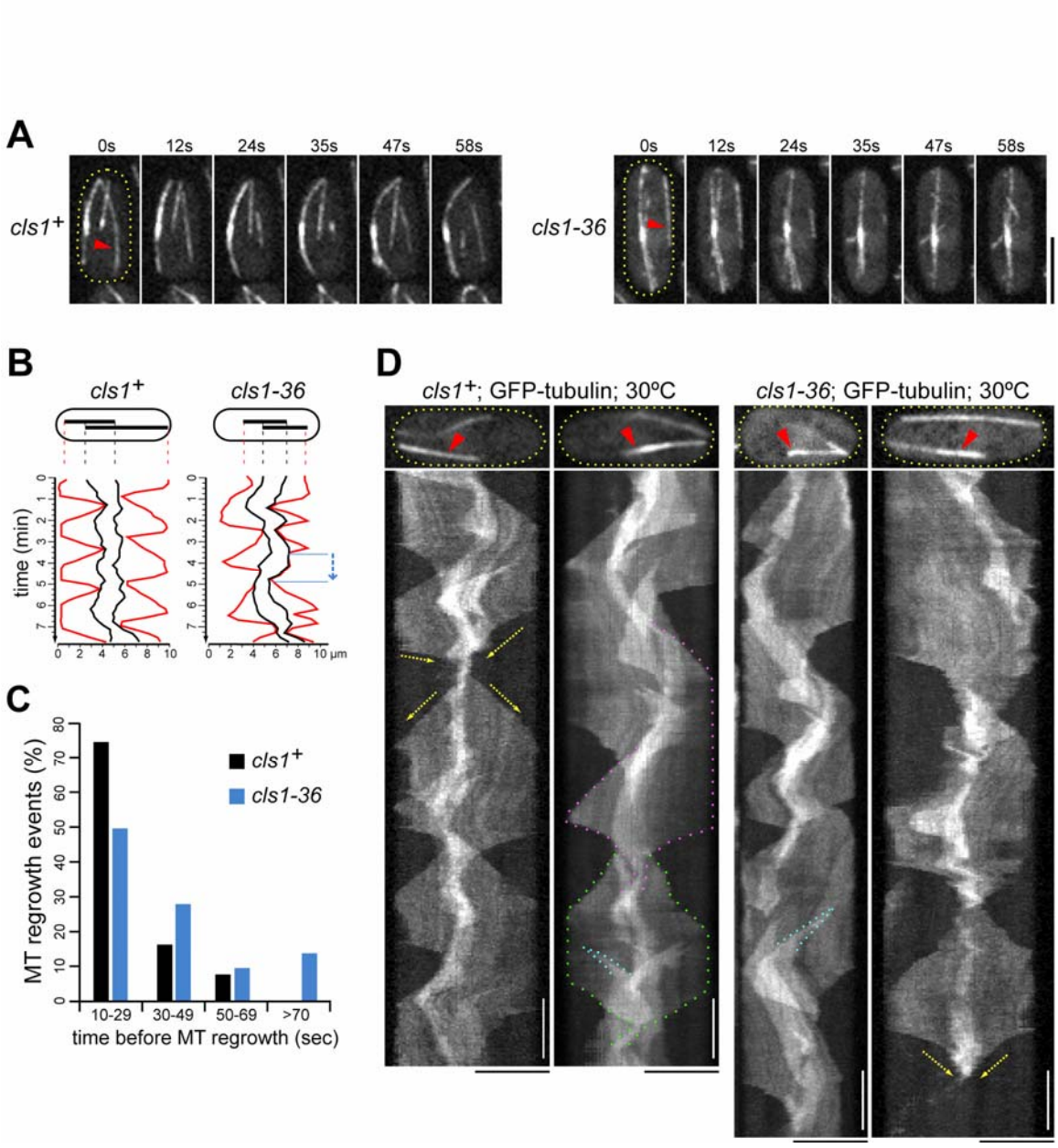

Figure S7. Interphase MT Defects in *cls1* Mutants

(A) Interphase MT bundle disassembly in *cls1*^{ts}. Cells expressing GFP-tubulin were imaged at 30ºC. The indicated bundles (red arrowheads) shrink down to <1µm stubs; the bundle is maintained in the wild-type cell and is lost in the *cls1-36* cell. Maximum projection confocal images are shown. Scale bar: 5µm.

(B) Single representative interphase MT bundles from wild-type or *cls1-36* cells imaged at 30ºC. Traces represent positions over time of plus ends (red) and boundaries of the overlap zone (black) within the cell. The blue arrow depicts the parameter measured in (C).

(C) Histogram of the time before a MT plus end regrows from an overlap zone. Mean values: 25±14 for *cls1*$^{+}$ (n=52 events in 5 cells); 39±27 for *cls1-36* (n=53 events in 5 cells); $P<0.01$.

(D) Cells expressing GFP-tubulin were imaged at 30ºC. Kymographs of the indicated bundle (red arrowheads) were constructed from single-plane confocal time-lapse images (0.5 fps). In both wild-type and *cls1-36*, MTs were nucleated along pre-existing MTs (blue outlines). But pause events (purple and green outlines) and stabilization of short regions of MT (yellow arrows; see also Figure 4B) were only seen in wild-type. Vertical scale bar: 1 min.

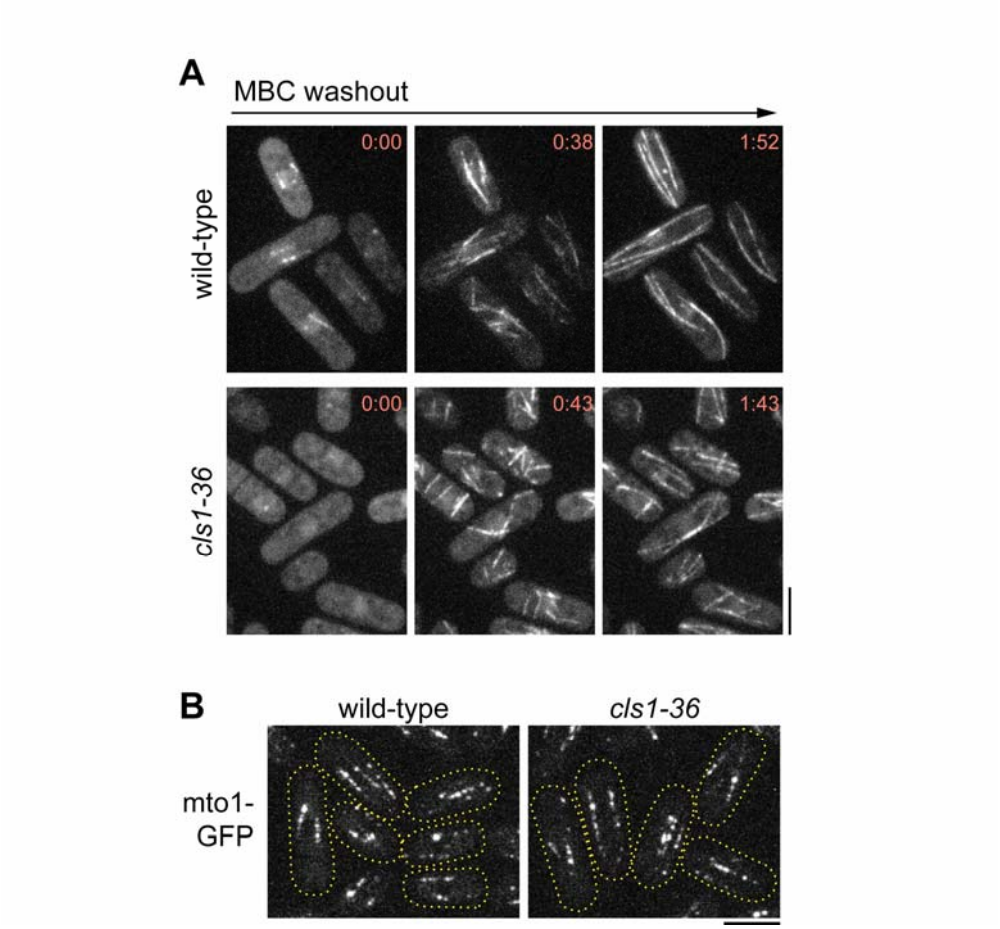

Figure S8. Cytoplasmic MT Nucleation in *cls1*

(A) Wild-type and *cls1-36* cells expressing GFP-tubulin were treated with 25µg/mL MBC at the restrictive temperature (36ºC) in a flow chamber. Stable MT stubs are maintained in wild-type cells in the presence of MBC. Upon washout of the drug, MTs regrew in both directions from the stable stubs and maintained the linear bundle organization. MBC treatment of *cls1-36* cells abolished most stubs, but washout of the drug still led to efficient MT regrowth. Most of these MTs were nucleated in the vicinity of the nucleus in apparently random orientations; the MTs were subsequently organized into linear bundles. Time after MBC washout is indicated in min:sec. Scale bar: 5µm.

(B) Mto1-GFP localization in wild-type (left) and *cls1-36* (right) interphase cells at 36ºC. In the *cls1* mutant cells, mto1p localizes normally to multiple dots (γ-tubulin complex satellites) along the interphase MT bundles.

Images are maximum projections of confocal stacks.

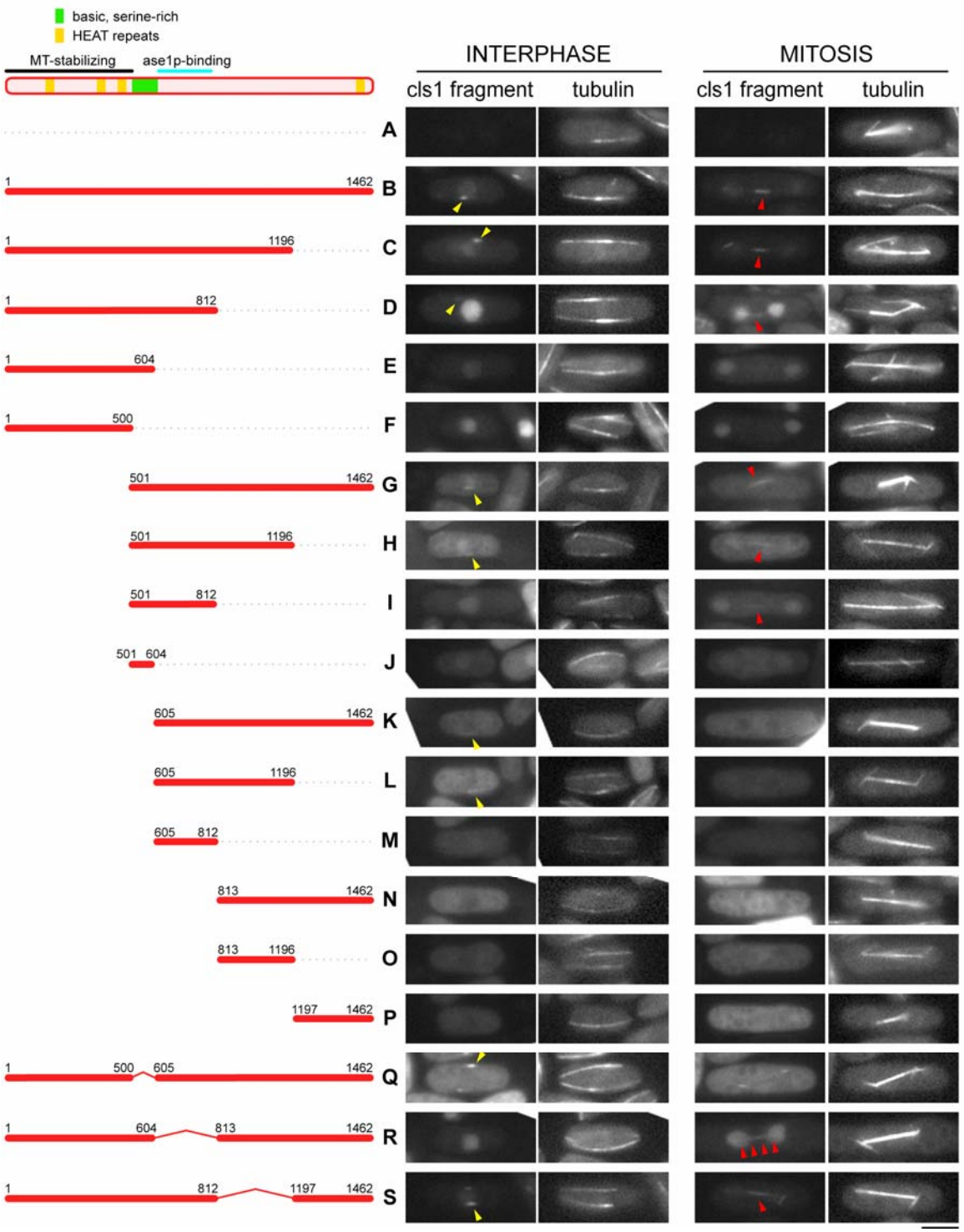

Figure S9. Intramolecular Determinants of cls1p Localization

The cls1p domains involved in targeting MTs were mapped by expressing mCherry fused to the indicated cls1 fragment (from plasmids) and GFP-tubulin (from an integrated *SV40* promoter) in *cls1*$^{+}$ haploid cells. The full-strength *nmt1* promoter that drove expression of the mCherry fusion

protein was repressed with thiamine. Expression levels of these fusion proteins, as determined by relative fluorescence intensity, often varied greatly depending on the cls1 fragment, so an effort was made to display cells with similar levels. Single-focal-plane wide-field images are shown. Full-length mCherry-cls1p localized normally to MT overlap zones in interphase and mitosis, but an abnormal localization to overlapping regions of cytoplasmic astral MT bundles was often present—this is likely explained by the high expression levels relative to endogenous cls1p. Other than full-length cls1p, many smaller fragments localized to MT overlap zones within interphase bundles (yellow arrowheads; B, C, D, G, H, K, L, Q, S) and the mitotic spindle (red arrowheads; B, C, D, G, H, I, S). Only the ase1p-binding domain was strictly required for targeting regions of overlapping MTs (R). Although the ase1p-binding domain did not localize by itself to regions of MT overlap, it helped direct neighboring sequences to these sites (I, L). Fragments lacking the MT stabilization domain (G, H), the basic domain (Q), or both (K, L) could still target interphase MT overlap zones. None of the fragments lacking the basic region localized to spindle MTs within the nucleus (K-Q), suggesting the presence of a nuclear import signal. Conversely, sequences in the C-terminus may be important for localizing cls1p to the cytoplasm (D, I). Scale bar: 5µm.

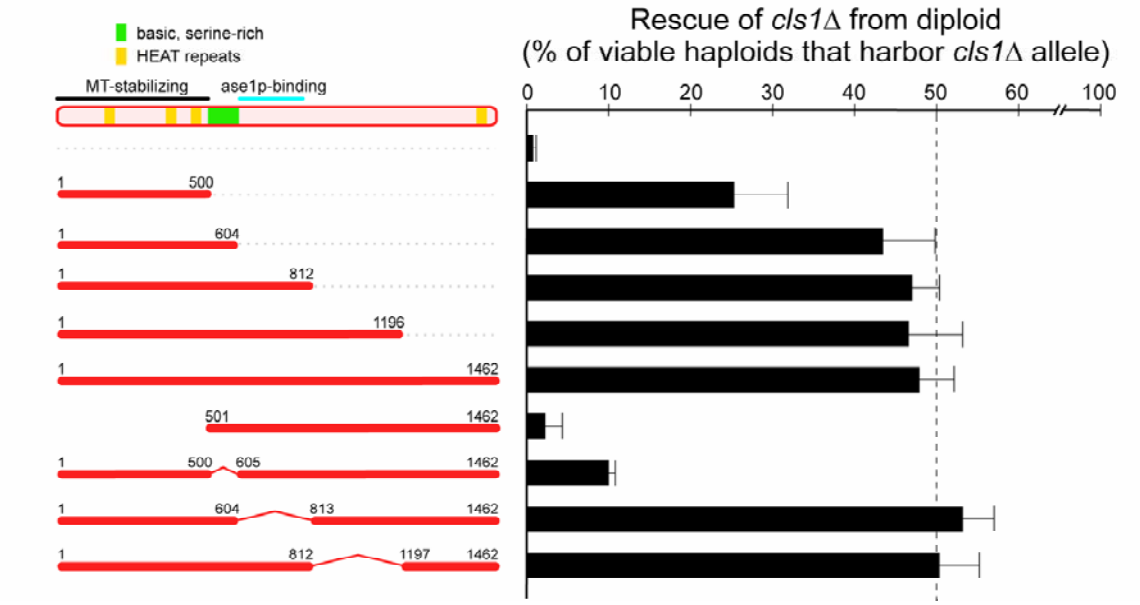

Figure S10. Rescue of Viability in *cls1*Δ by cls1 Fragments

Haploid spores were isolated from a *cls1*Δ/*cls1*$^{+}$ diploid strain (SB575) harboring plasmids with the indicated cls1 fragments. The plasmids encode cls1 fragments fused to the C-terminus of mCherry, and expression of the fusion protein was driven by a full-strength *nmt1* promoter in the repressed condition. The percent of viable spores that contained the *cls1*Δ allele is shown. Fifty percent is the hypothetical maximum for full rescue of viability. Results are from three independent experiments.

Error bars indicate SD.

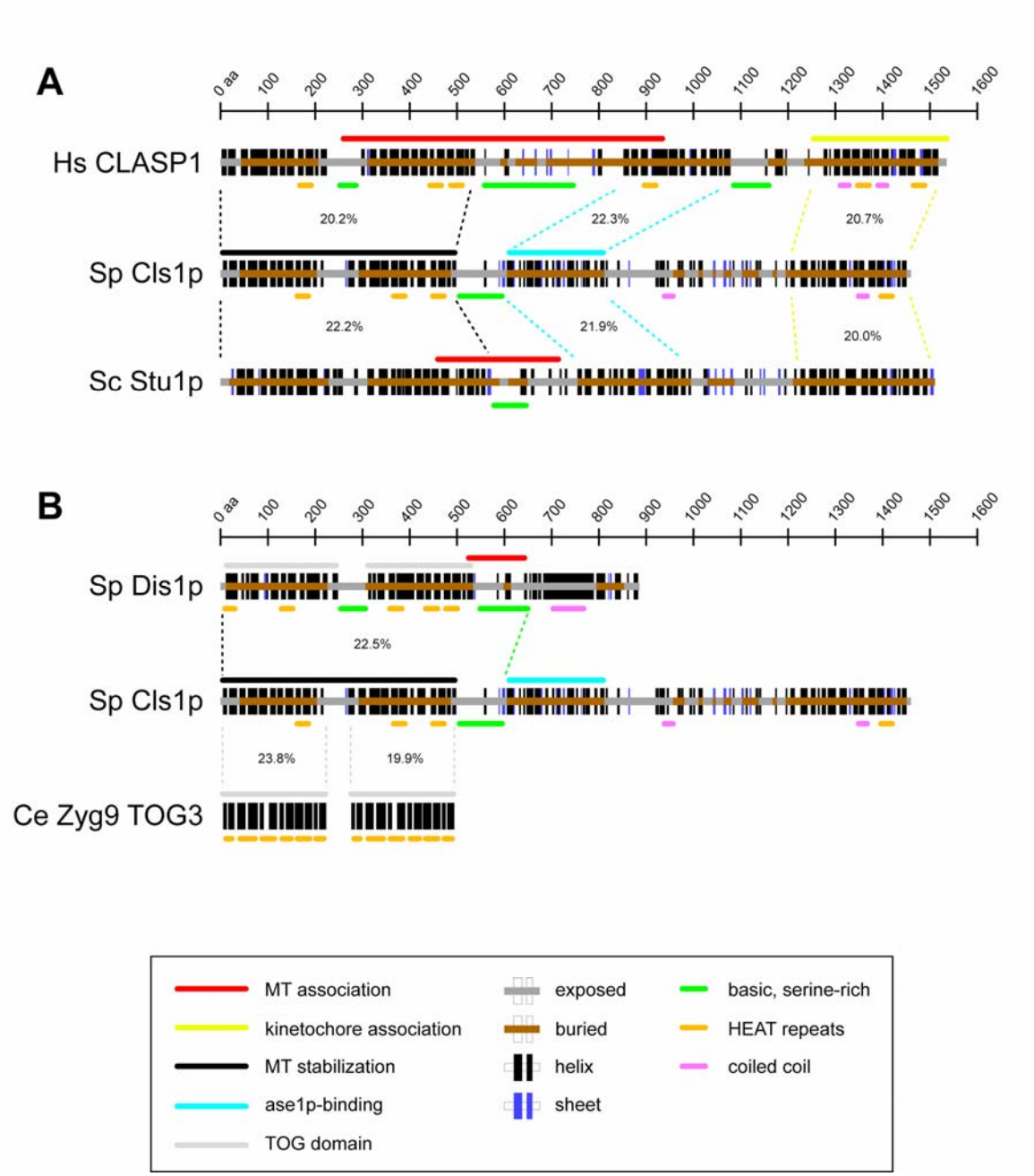

Figure S11. Cls1p Homology to Other CLASPs and to the dis1/TOG Family

(A) Cls1p has conserved domain architecture with other CLASP proteins. Within Hs CLASP1, aa 250-943 (red) and aa 1256-1538 (yellow) are sufficient for association *in vivo* with MTs and kinetochores, respectively (Maiato et al., 2003). Within Sc Stu1p, aa 461-716 (red) are required for MT binding *in vitro* (Yin et al., 2002). Dotted lines indicate regions that contain both

sequence homology and predicted structural similarity with known functional domains: Sp Cls1p MT-stabilizing domain (aa 1-500, black); Sp Cls1p ase1p-interacting domain (aa 605-812, light blue); and Hs CLASP1 kinetochore-associating domain (aa 1256-1538, yellow).

Sp Cls1p aa 1-500 vs. Hs CLASP1 aa 1-540: 20.2% identity, score=168.

Sp Cls1p aa 1-500 vs. Sc Stu1p aa 1-561: 22.2% identity, score=316.

Sp Cls1p aa 605-812 vs. Hs CLASP1 aa 854-1065: 22.3% identity, score=30.

Sp Cls1p aa 605-812 vs. Sc Stu1p aa 794-996: 21.9% identity, score=47.

Sp Cls1p aa 1197-1462 vs. Hs CLASP1 aa 1256-1538: 20.7% identity, score=36.

Sp Cls1p aa 1197-1462 vs. Sc Stu1p aa 1216-1513: 20.0% identity, score=30.

(B) The N-terminus of cls1p shares common features with dis1/TOG proteins. Conservation of amino acid sequence between these protein families has previously been noted (Lemos et al., 2000). Within Sp Dis1p, aa 518-645 (red) are required but not sufficient for MT binding *in vitro* (Nakaseko et al., 1996). The structure of the TOG3 domain of Ce Zyg9 is known (Al-Bassam et al., 2007). Dotted lines indicate regions that contain both sequence homology and predicted structural similarity with known functional domains: Sp Cls1p MT stabilization and basic domains (aa 1-604, black and green); Ce Zyg9 TOG3 (aa 647-866, light gray).

Sp Cls1p aa 1-604 vs. Sp Dis1p aa 1-655: 22.5% identity, score=164.

Sp Cls1p aa 1-218 vs. Ce Zyg9 aa 647-866: 23.8% identity, score=60.

Sp Cls1p aa 275-499 vs. Ce Zyg9 aa 647-866: 19.9% identity, score=21.

Sp Dis1p aa 5-225 vs Ce Zyg9 aa 647-866: 21.1% identity, score=79; not shown.

Sp Dis1p aa 308-531 vs Ce Zyg9 aa 647-866: 21.1% identity, score=82; not shown.